SUPERHYDROPHOBIC TO SUPERHYDROPHILIC WETTABILITY TRANSITION OF FUNCTIONALIZED SiO_2 NANOPARTICLES

L. G. Arellano-Galindo
A. C. Reynosa-Martínez
J. R. Gaitán-Arévalo
M. F. Valerio-Rodríguez
G. Vargas-Gutiérrez
E. López-Honorato

Work sponsored by a grant from the Secretaría de Energía and Consejo Nacional de Ciencia y Tecnología (SENER-CONACYT) as part of the Mexican Center for Innovation in Ocean Energy (CEMIE-Océano, project number 249795).

Notice: This manuscript has been authored by UT-Battelle, LLC, under contract DE-AC05-00OR22725 with the US Department of Energy (DOE). The US government retains and the publisher, by accepting the article for publication, acknowledges that the US government retains a nonexclusive, paid-up, irrevocable, worldwide license to publish or reproduce the published form of this manuscript, or allow others to do so, for US government purposes. DOE will provide public access to these results of federally sponsored research in accordance with the DOE Public Access Plan (http://energy.gov/downloads/doe-public-access-plan).

Superhydrophobic to Superhydrophilic Wettability Transition of Functionalized SiO_2 Nanoparticles

Lilia Guadalupe Arellano-Galindo[a], Ana Cecilia Reynosa-Martínez[a], Juniet Rebeca Gaitán-Arévalo[a], María Fernanda Valerio-Rodríguez[a], Gregorio Vargas-Gutiérrez[a], Eddie López-Honorato[a,b*]

[a] Centro de Investigación y de Estudios Avanzados del IPN (Cinvestav), Unidad Saltillo. Av. Industria Metalúrgica 1072, Parque Industrial Saltillo Ramos Arizpe, Ramos Arizpe, Coahuila, 25900

[b] Oak Ridge National Laboratory, Oak Ridge, TN 37831, United States.

Abstract

The superhydrophobic and superhydrophilic surfaces and their transitions are of great interest for the production of self-cleaning, anti-biofouling, or corrosion-resistant materials. This work reports the wettability transition from superhydrophobic to superhydrophilic SiO_2 nanoparticles functionalized with 1H, 1H, 2H, 2H-perfluorooctyltriethoxysilane (POTS) and induced by temperature. The functionalization of these nanoparticles was confirmed by Fourier transform infrared spectroscopy, X-ray photoelectron spectroscopy (XPS), and transmission electron microscopy. The functionalization of SiO_2 nanoparticles with POTS resulted in superhydrophobic surfaces with water contact angles up to 157°. A sudden transition to superhydrophilic behavior with water contact angles (WCA) below 5° was observed when the sample was heat-treated at 500 °C, despite the presence of fluorine on the surface of these

* Corresponding author: E-mail: honoratole@ornl.gov
These authors contributed equally: Lilia Guadalupe Arellano-Galindo and Ana Cecilia Reynosa-Martínez.

nanoparticles, as confirmed by XPS and transmission electron microscopy. XPS suggested that the transition was caused by the change in orientation of the fluoroalkyl molecules and its partial decomposition due to the loss of the -CF_3 group, resulting in shorter chains with a tail-end group with C-O bonds, which promoted the superhydrophilicity.

Keywords: Interfaces, surfaces, SiO_2, functional applications

1. Introduction

The control of superwettability of solid surfaces is of great interest to the nuclear and renewable energy industry due to the versatility of applications such as anti-corrosion, anti-icing, drag reduction, self-cleaning, antibacterial, and anti-biofouling [1-7]. Because the wettability of a solid depends on the morphology and chemistry of its surface [8], it is possible to obtain superwettability properties such as superhydrophobicity, in which the WCA is >150°, or superhydrophilicity, in which the liquid droplet spreads over the surface with a WCA less than 5° [9, 10]. Although hydrophobicity and hydrophilicity are opposite properties, the transition between them can occur. This type of surface transition has been reported mainly on transition-metal oxide surfaces such as ZnO, CuO, and WO_3, as well as aluminum coated with polydimethylsiloxane, silicon coated with poly(N-isopropyl acrylamide), and in Al_2O_3/silica (SiO_2) fiber membranes [5, 9-14]. In some cases, this transition occurs because of adsorbed contaminants on the surfaces, surface degradation, or a change in the chemical composition in response to stimuli such as light, electricity, temperature, and pH [3, 14, 15].

Silica (SiO_2) is a ceramic material widely used for the manufacture of surfaces that are by nature hydrophilic due to the high density of Si-OH groups. However, these surfaces can undergo a transition to superhydrophobic when the temperature is increased between 700 and 800 °C,

because these groups react with each other, giving rise to Si-O-Si bonds, which are hydrophobic [16, 17]. Another way to control the wettability of SiO_2 is through its surface chemistry during its synthesis because a surface with a greater number of Si-$(CH_3)_3$ groups can be obtained by controlling the molar ratio between trimethylethoxysilane and tetraethoxysilane (TEOS) during SiO_2 synthesis, obtaining a WCA of 151° [18].

Additionally, the functionalization of SiO_2 with molecules such as hexadecyl polysiloxane, (3-amino-propyl)triethoxysilane, chlorotrimethylsilane, and dichlorodimethylsilane has been widely used to obtain superhydrophobic surfaces because these molecules significantly reduce the surface energy [19-22]. Superhydrophobic surfaces can also be obtained using fluoroalkyl silanes since the presence of the -CF_3 group reduces the surface energy to 6.7 mJ/m^2 [23]. For example, Liu et al. reported the functionalization of a glass substrate with heptadecafluoro-1, 1, 2, 2-tetrahydrodecyltrimethoxysilane that showed a WCA of 169° [24], whereas 1H, 1H, 2H, 2H-perfluorooctyltriethoxysilane, used for the functionalization of SiO_2 nanoparticles, had a WCA of 161° [25]. On the other hand, chain orientation has also been reported to affect the wettability of the POTS functionalized surface, since the packing of the -CF_3 groups in the outermost layer of the coating was modified until reaching a WCA of 123° [23]. Although fluoroalkyl silanes are effective for the production of superhydrophobic surfaces, it has been observed that they can decompose at low annealing temperatures. For example, Yang et al. studied the thermal stability of a monolayer of POTS on a SiO_2 substrate with a WCA of 108° before heat treatment and noted its decomposition at an annealing temperature of 100–150 °C and the loss of the -CF_2 and -CF_3 groups [26, 27].

In this work, the temperature-induced surface transition of SiO_2 nanoparticles functionalized with a fluoroalkyl silane molecule was studied. The SiO_2 nanoparticles were synthesized by the sol-gel and functionalized with POTS and deposited on a glass frit. These coatings produced a

WCA of 157°; however, after heat treatment at 500 °C, the surface transitioned to superhydrophilic with a WCA of <5°. This transition was correlated to the partial loss of fluorine in the form of CF_3-CF_2, CF_2-CF_2, and CF_2-CH_2 and the subsequent formation of C-O bonds as observed by X-ray photoelectron spectroscopy (XPS), in addition to the change in orientation of the POTS molecules due to its degradation.

2. Experimental

2.1 Materials preparation

The SiO_2 nanoparticles were produced using TEOS (98%, Sigma-Aldrich), hydrochloric acid (28.3%, Fraga Lab), deionized water, ethanol (99%, Sumilab), and ammonium hydroxide (NH_4OH, 28.3%, Jalmek) [28]. Initially, 4 ml of ethanol were mixed with 4 ml of deionized water, 5 ml of TEOS, and stirred for 20 min. Subsequently, 2 ml of hydrochloric acid was added, continuing the stirring for 5 min. Then 2 ml of NH_4OH were added, leaving it under stirring for 2 h at 60 °C. The powders were then separated by centrifugation with ethanol, using a molar ratio of 0.3 at 2000 rpm. Finally, the powder was dried at 80 °C for 24 h and milled in an agate mortar.

The SiO_2 nanoparticles were functionalized using POTS (98%, Sigma-Aldrich). Initially, 34 ml of toluene (99.8%, Sigma Aldrich) and 22 ml of dichloromethane (99.5%, Jalmek) were mixed in a three-necked round bottom flask with 4 g of SiO_2 nanoparticles and left under stirring for 15 min. Subsequently, 1 ml of POTS was added dropwise. The mixture was left under constant stirring for 20 h and then centrifuged at 4000 rpm. The nanoparticles were washed three times with dichloromethane using a molar ratio of 0.5 at 4000 rpm. The washed particles were finally dried at 60 °C for 24 h. The POTS functionalized nanoparticles (NPOTS) were deposited over a glass frit, using 1 µg of NPOTS sprayed over an area of 6 cm^2. All the samples prepared had the same amount

of material per area. Finally, the samples were heat-treated for 1 h in air at 200, 300, 400, and 500 °C with a heating ramp of 10 °C/min.

2.2 Characterization

The SiO_2 nanoparticles were characterized by scanning electron microscopy using a Phillips XL30SEM microscope and by transmission electron microscopy (TEM) using a JEOL JEM F200. Particle size was measured using the software ImageJ. The functional groups were characterized by Fourier transform infrared spectroscopy (FTIR) in a PerkinElmer Frontier FTIR/NIR, which has an accessory of diffuse reflectance from 4000 to 400 cm^{-1}, a resolution of 4 cm^{-1}, and an accumulation of 30 sweeps. Additionally, samples were characterized by XPS Thermo Scientific K-Alpha with a 1.9×10^{-7} mbar vacuum chamber and an aluminum anode as X-ray monochromatic source with a radiation energy of 1486.68 eV, and calibrating the binding energy using the carbon energy at 284 eV. Thermal stability was evaluated by thermogravimetric analysis (TGA) in a TGA thermal analyzer (TA Instruments, model SDT Q600) with argon atmosphere and a heating rate of 10 °C/min. The contact angles were measured using an in-house-built goniometer based on the ASTM E 165-95 norm "Standard Test Method for Liquid Penetrant Examination", and ImageJ software was used for the WCA measurement [29]. Finally, the surface area was measured by the Brunauer–Emmett–Teller (BET) analysis with an Autosorb iQ Series from Quantachrome Instruments with nitrogen gas.

3. Results and Discussions

3.1. Characterization of SiO_2 nanoparticles

Figure 1 shows the FT-IR spectrum of the SiO_2 nanoparticles obtained by sol-gel. A broad and intense band is observed at 3148 cm^{-1}, corresponding to the stretching vibrational modes of -OH,

which could be attributed to the Si-OH group [30]. Two bands at 3032 and 2812 cm^{-1} were also observed, which could be assigned to the symmetric and asymmetric vibrational modes of the methyl group ($-CH_3$), probably originating from the $–SiOCH_3$ group (Figure S1) [31]. At 1632 cm^{-1}, a band corresponding to the flexion vibrational mode of water was also observed [22]. Additionally, the band at 1403 cm^{-1} was also assigned to the flexion vibrational mode of the $-CH_3$ group [32]. Furthermore, at 966 cm^{-1}, a band could be observed corresponding to the Si-OH group. Finally, the bands at 796 and 468 cm^{-1} could be attributed to the asymmetric stretching vibrational mode of the Si-O-Si group [18, 31].

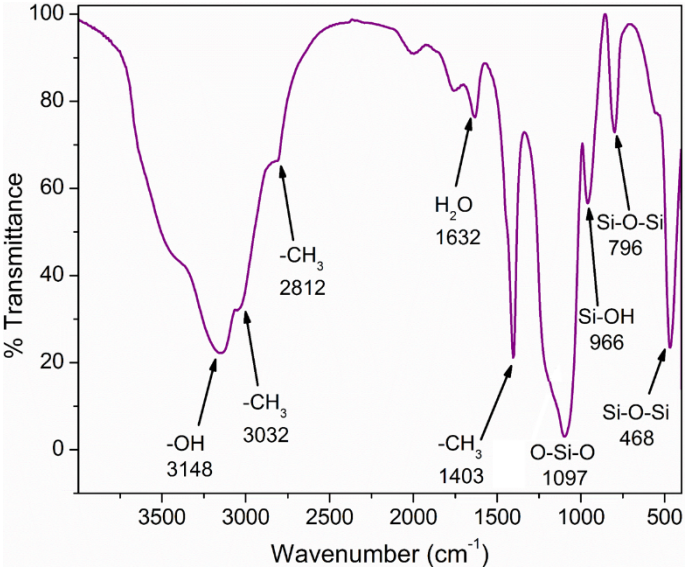

Figure 1. FTIR spectrum of SiO_2 nanoparticles synthesized by sol-gel.

Figure 2 shows the TEM micrographs of the SiO_2 nanoparticles produced. The nanoparticles were mostly spherical with a diameter between 20 and 160 nm. Figure 2b shows that the nanoparticles were partially aggregated with a surface area of 85.31 m^2/g, which is higher than the value reported by Diedrich et al., who synthesized SiO_2 nanoparticles with a diameter of 101 nm and a surface area of 57 m^2/g [33].

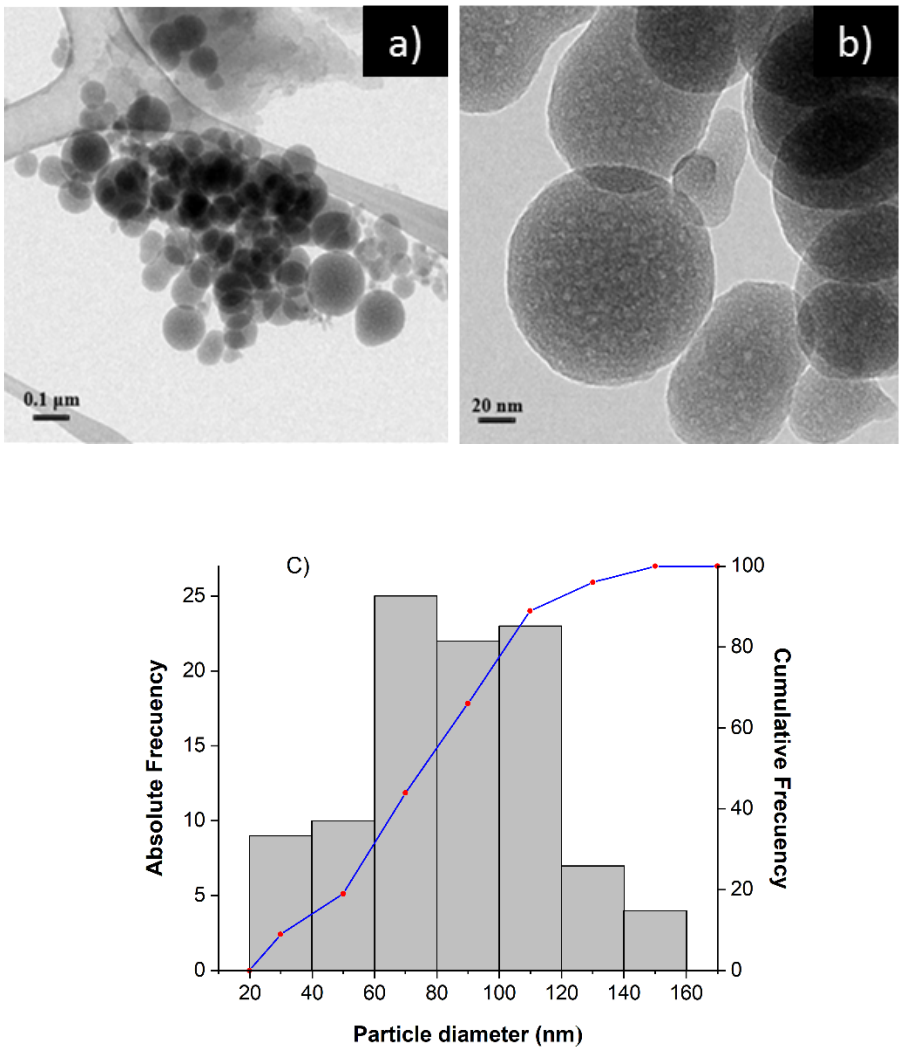

Figure 2. TEM micrographs of SiO_2 nanoparticles synthesized by sol-gel and their particle size distribution.

3.2. Functionalization of SiO_2 Nanoparticles

Figure 3a shows the FTIR spectra of SiO_2 nanoparticles functionalized with POTS (NPOTS). The bands previously described corresponding to the SiO_2 nanoparticles at 3139, 2989, 2898, 1404, 1078, 955, 801, 452 cm^{-1} were maintained. Additionally, the signal corresponding to the Si-O-Si group at 1078 cm^{-1} had a more pronounced shoulder, possibly caused by the presence of a new band close to 1200 cm^{-1}, where the vibrational modes of the stretching and wagging for

the -CF bonds are present [25, 32, 34]. Notably, the intensity of the -OH group at 3139 cm^{-1} also decreased, possibly due to the interaction between the SiO_2 nanoparticle and the POTS molecule because the functionalization occurs on this functional group [35].

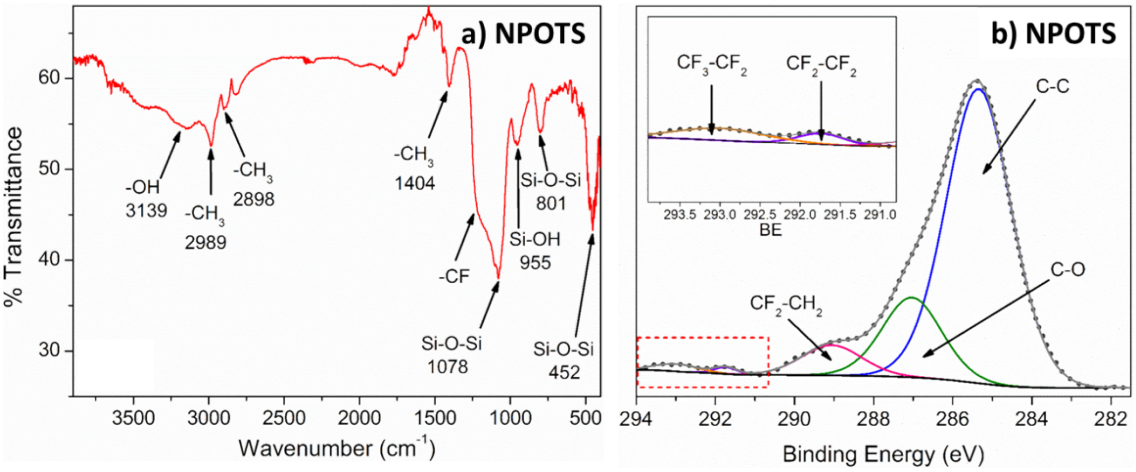

Figure 3. a) FT-IR spectra of as-produced functionalized nanoparticles with POTS (NPOTS) and b) High-resolution XPS spectra of the C1s region of NPOTS.

Figure 3b depicts the high-resolution XPS spectra of the C1s region for NPOTS without heat treatment, showing the presence of C-F bonds and thus confirming the functionalization of the SiO_2 nanoparticles with fluoroalkyl silanes. As can be observed in Figure 3b, the bands associated with the C-C, C-O, CF_2-CH_2, CF_2-CF_2, and CF_3-CF_2 bonds were present at 285.1 ±0.3, 287.1 ±0.4, 289.4 ±0.2, 292.0 ±0.4, and 293.1 ±0.3 eV, respectively [30] (see Figure S2 for the structural representation of the POTS molecule). Table 1 shows that the C-C bond had a content of 73.3%, and the C-O bond content was 18.0%, whereas the CF_2-CH_2 and CF_2-CF_2, and -CF3 bonds belonging to the POTS fluoroalkyl silane chain had concentrations of 6.9, 0.6%, and 1.2%, respectively [26, 31].

Table 1. Quantification of bonds by XPS on the surfaces coated by NPOT without heat treatment.

	C-C	C-O	CF_2-CH_2	CF_2-CF_2	CF_3-CF_2
NPOTS	73.3	18.0	6.9	0.6	1.2

3.3. Wettability transition

SiO_2 nanoparticles without any functionalization had a water contact angle of 28.9° ±3.3° (Table 2 and Figure S3). A considerable increase in WCA was observed when the SiO_2 nanoparticles were functionalized and heat-treated at 200 °C, reaching values of 157 ° (Table 2 and Figure S4a). These values were similar to the ones reported by Wu et al., who obtained values of 161° [25]. This superhydrophobic behavior was attributed to the fluorine atoms present in the molecules of the fluoroalkyl silanes, as they tend to provide a low-surface-energy of 6.7 mJ/m^2 because of the ordering of the fluoroalkyl silanes with their molecular axis perpendicular to the SiO_2 surface [1, 24, 34].

Table 2. Water contact angle of NPOTS heat-treated at 200, 300, 400, and 500 °C.

	200 °C	300 °C	400 °C	500 °C
NPOTS	157° ± 4.3	157° ± 7.5	159° ± 4.7	<5°

Table 2 shows that the superhydrophobicity of this material was maintained when samples were heat-treated up to 400 °C by maintaining a WCA of around 157–159°. However, when the sample was heat-treated at 500°C, its WCA dropped to less than 5° (superhydrophilic) because measuring the WCA was no longer possible since the droplet quickly spread (Figure S4b).

Figure S5 shows the FTIR spectra of the surface coated with the functionalized nanoparticles after heat treatment at 200 °C (Figure S5a) and 500 °C (Figure S5b). It can be seen

that after heat treatment the nanoparticles remained functionalized because the band at 1090 cm^{-1} can still be observed. This band corresponds to the Si-O-Si bond from the core of the nanoparticle of SiO_2. However, as previously mentioned, this band seems to overlap with another band at ~1078 cm^{-1}, which is related to the -CF bonds (See Figure 3) [35].

Figure 4 shows the TEM micrograph and elemental mapping of NPOTS heat-treated at 500 °C. The elemental mapping shows the presence of Si, O, C, and even F. TEM showed that the samples transitioned from superhydrophobic to superhydrophilic even when F was retained on the sample. Because the presence of F is considered to be the origin of the superhydrophobicity of this type of particle, further tests were performed to understand the origin of this wettability transition.

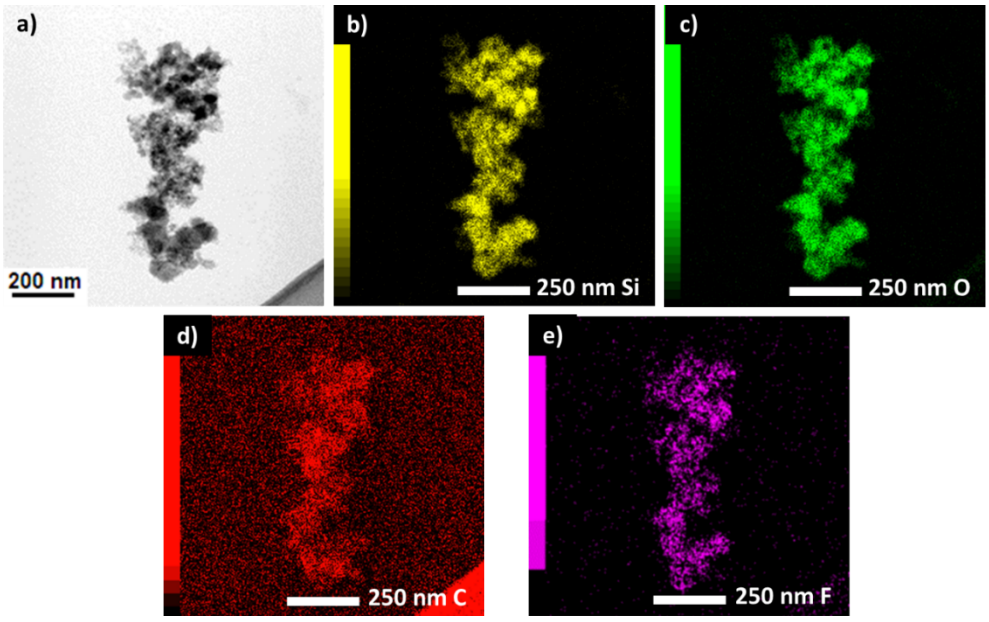

Figure 4. Micrographs and elemental mapping obtained from TEM showing the distribution of the elements in NPOTS heat-treated at 500 ° C.

The thermal stability of the functionalized particles was also evaluated by TGA. Figure 5 shows the TGA curve of NPOTS, where a weight loss of 40% at 160–262 °C was observed.

Previous studies have suggested that between 30 °C and 200 °C a weight loss occurs due to water desorption; however, the loss of molecule fragments with low cross-linking has also been reported [36, 37]. Therefore, this weight loss could be attributed not only to the desorption of water but also to the loss of -OH groups from the SiO_2 that were not functionalized [33, 36]. Additionally, a 5% weight loss was observed up to 522 °C, which could be due to the breakdown of the fluoroalkyl silane. Previous reports have suggested that these molecules start their decomposition around 300 °C at the methylene chain [27, 37]. Although it has been suggested that most fluoroalkyl silanes decompose at around 497 °C [36], the results of the authors' study show that the NPOTS continued its decomposition up to 522 °C, which could explain why at 500 °C the sample still contained F as observed by TEM in Figure 5.

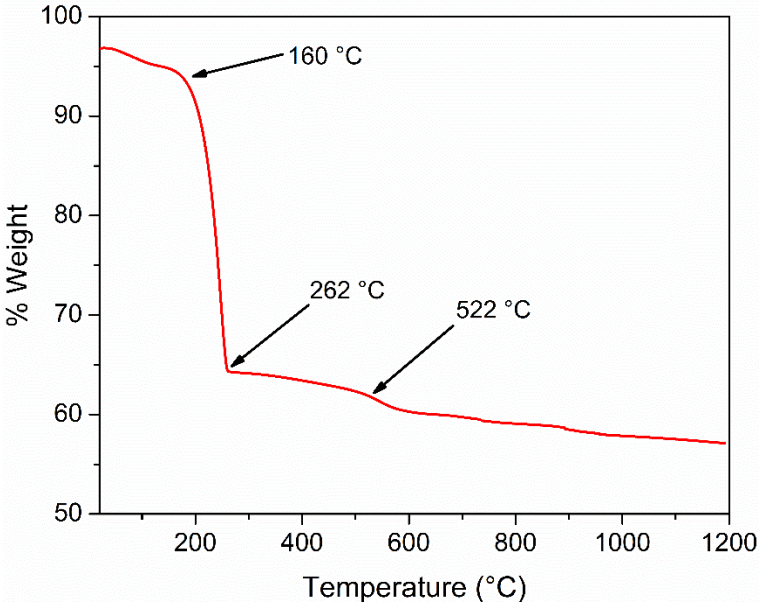

Figure 5. Thermogravimetric curves of NPOTS.

Figure S6 shows the wide XPS spectra of the as-produced, and heat-treated NPOTS at 200 and 500 °C. The presence of silicon (Si 2p/2) can be observed in the region of 100–103 eV—carbon

(C 1s) between 284–286 eV, oxygen (O 1s) in 531–534 eV, and fluorine (F 1s) in 686–689 eV. The presence of Si and O is attributed to the SiO_2 nanoparticles, whereas C and F originate from the POTS molecule [28, 38]. Figure 7 shows the high-resolution XPS spectra of the C1s region of NPOTS heat-treated at 200 and 500 °C. NPOTS particles heat-treated at 200 and 500 °C (Figure 7 and Table 3) showed a very similar C-C bond concentration of 90.5% and 85%, respectively. Conversely, the C-O bond showed a decrease after being heat-treated at 200 °C from 18.0% to 3.8%, compared with the as-produced material, but it had a slight increase when heat-treated at 500 °C up to 10.6% C-O. On the other hand, the CF_2-CH_2 bond decreased from 6.9% to 4.2% and 4.1%, when heat-treated at 200 and 500°C. Additionally, the CF_3-CF_2 bonds almost disappeared as the sample was heat-treated at 500 °C. Furthermore, the F1s region (Figure S7) showed that the two bands at 686 eV which correspond to the (-$CHFCH_2$)n bonds [38] and the band at 690 eV, which is attributed to the (CF_2-CF_2)n bonds, shifted toward 691 eV after the sample was heat-treated at 200 and 500°C [27, 39, 40]. This displacement was also reported by Hattori et al., who observed the band´s displacement from 686.1 to 688.7 eV due to the increase in temperature from 30 to 200° C [41]. Finally, at 500 °C, only one band at 691 eV (Figure S7c) was observed, which is assigned to the covalent F [39] probably due to the decomposition of the fluoroalkyl silane that result in a shorter chain (CF_2-CF_2)n. This behavior was also reported by An et al., who observed the band displacement to 691 eV when the sample was heat-treated above 200° C [39].

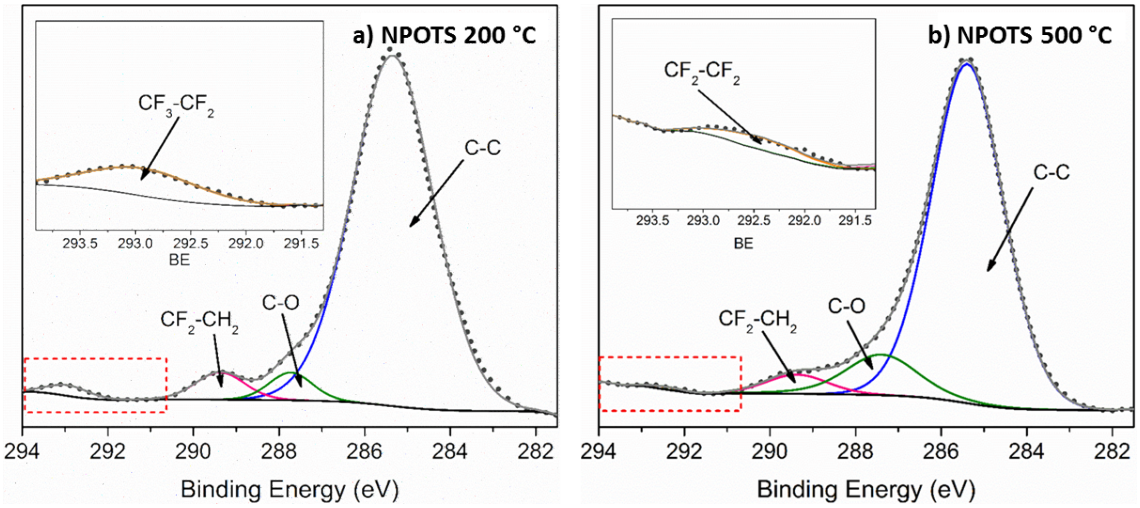

Figure 7. High-resolution XPS spectra of the C1s region of NPOTS, heat-treated at a) 200 °C and b) 500 °C.

Table 3. Quantification of bonds by XPS of NPOTS. Without heat treatment and treated at 200 and 500 ° C.

	C-C	C-O	CF_2-CH_2	CF_2-CF_2	CF_3-CF_2
NPOTS 200 °C	90.5	3.8	4.2	0	1.4
NPOTS 500 °C	85	10.6	4.1	0	0.3

These results suggest that the heat treatment, even at temperatures up to 500 °C, did not result in the total desorption of the fluoroalkyl chain since F was detected by TEM and XPS. Instead, the POTS molecules suffered from a partial decomposition by losing primarily the CF_3-CF_2 groups. Furthermore, the shift in the position of the (CF_2-CF_2)n band suggests that the molecule also changed in orientation and possibly was no longer in a perpendicular position with the SiO_2 nanoparticle, as suggested by Cai et al. [23]. This partial decomposition is similar to that reported by Yang et al. and Fréchette et al. [26, 27]. Additionally, although it has been reported

that most fluoroalkyl silanes decompose at around 375 °C, some -CF_x groups can remain stable up to 700 °C [36]. This shortening of the fluoroalkyl chain is of great relevance for the wettability of the surface because longer chains tend to be more hydrophobic. For example, Hozumi et al. observed that a fluoroalkyl silane with seven -CF_2 groups and the tail-end group -CF_3 achieved a WCA of 112°, whereas a fluoroalkyl silane without -CF_2 groups but still with the tail-end group -CF_3 achieved a WCA of 86° [31, 42]. Therefore, the reduction in WCA and the transition from superhydrophobic to superhydrophilic could be partially explained by the partial decomposition of the fluoroalkyl silane molecule and its change in orientation, because the -CF_3 bond (lost at 500°C), the length of the -CF_2 chain, and the orientation of the molecule are important to achieve a superhydrophobic behavior. However, although a reduction in WCA could have been expected, the reach of a superhydrophilic behavior with the presence of F is still not clear. XPS suggests that at 500 °C, the surface of the particles increased their content of C-O bonds, which could be attributed to the partial oxidation of the molecule. It is possible that this increase in hydrophilic bonds could be partially responsible for the increase in hydrophilicity, since they are capable of increasing the surface energy and form hydrogen bonds with water [43, 44].

On the other hand, Figure 8 shows the impact of heat treatment on the microstructure of NPOTS. Figure 8a shows that at 200°C the nanoparticles were agglomerated most likely due to the presence of the fluoroalkyl silane, which resulted in the formation of a rough surface with pores from 200 nm to several micrometers. However, as the sample was heat-treated at 500 °C (Figure 8b), the nanoparticles appeared to be more clearly defined, most likely due to the partial decomposition of the POTS molecules, while maintaining a rough surface. Therefore, it is likely that the transition from superhydrophobic to superhydrophilic could be related to the change of surface chemistry (an increase of C-O and Si-O bonds) while maintaining a rough surface that

would promote the formation of a stable Cassie-Baxter state, which favors extreme wetting conditions (superhydrophobic and superhydrophilic) [45, 46].

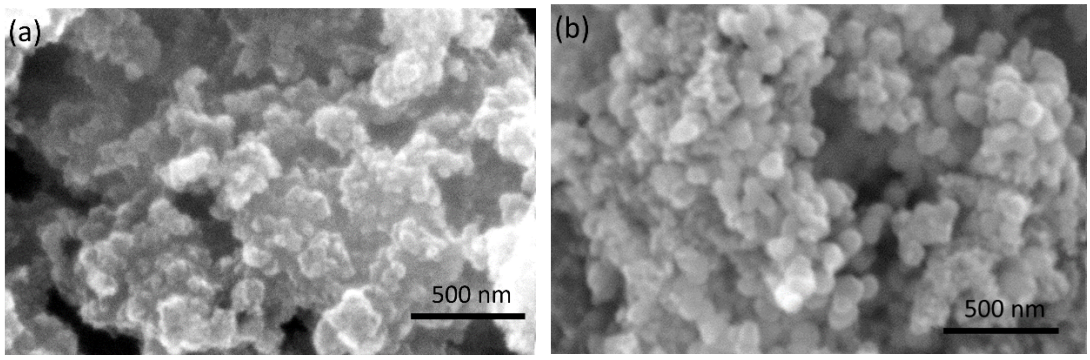

Figure 8. SEM micrographs of SiO_2 nanoparticles functionalized with POTS after heat treatment at (a) 200 and (b) 500°C.

4. Conclusions

The functionalization of SiO_2 nanoparticles with the POTS molecule results in superhydrophobic surfaces with a WCA of 157°. However, the transition to a superhydrophilic surface was achieved as the sample was heat-treated up to 500 °C. At this temperature, the bonds CF_2-CH_2, CF_2-CF_2, and CF_3-CF_2 are gradually lost, which results in a shorter chain that loses its superhydrophobic properties. The results of this study show that although the full decomposition of POTS occurs up to 522 °C, the molecule possibly undergoes oxidation because XPS detected an increment in C-O bonds by 10.6%. Additionally, SEM images showed that even at 500°C the surface roughness of the material was maintained. Therefore, it is likely that the superhydrophobic to superhydrophilic transition originated from a change in surface energy induced by the presence of more C-O and Si-O bonds, in conjunction with a rough surface, which promoted a stable Cassie-Baxter state.

5. Acknowledgments

This work was supported by a grant from the Secretaría de Energía and Consejo Nacional de Ciencia y Tecnología (SENER-CONACYT) as part of the Mexican Centre for Innovation in Ocean Energy (CEMIE-Océano, project number 249795). The authors would like to acknowledge CONACYT for the MSc and PhD scholarships awarded to Lilia Arellano Galindo, Juniet Gaitan Arevalo, María Fernanda Valerio-Rodríguez, and Ana Cecilia Reynosa-Martínez.

References

[1] L. Feng, Z. Zhang, Z. Mai, Y. Ma, B. Liu, L. Jiang, D. Zhu, A super-hydrophobic and super-oleophilic coating mesh frilm for the separatioin of oil and water, Angewandte Chemie, 43 (2004) 2012-2014.

[2] K. Han, P.T. Y., K. Yong, H.J. Cha, Combinational biomimicking of lotus leaf, mussel, and sandcastle worm for robust superhydrophobic surfaces with biomedical multifunctioinality: antithrombotic, antibiofouling, and tissue closure capabilities, ACS Applied Materials and Interfaces, 11 (2019) 9777-9785.

[3] X. Li, W. G., A.S. Moita, C. Zhang, S. Wang, Y. Liu, Fabrication of bio-inspired non-fluorinated superhydrophobic surfaces with anti-icing property and its wettability transformation analysis, Applied Surface Science, 505 (2020) 144386.

[4] S. Wang, K. Liu, X. Yao, L. Jiang, Bioinspired surfaces with superwettability: new insight on theory, design, and applications, Chemical Reviews, 115 (2015) 8230-8293.

[5] Z. Li, T. Shi, T. Zhang, Q. Guo, F. Qiu, X. Yue, D. Yang, Hierarchical Al_2O_3/SiO_2 fiber membrane with reversible wettability for on-demand oil/water separation, Korean Journal of Chemical Engineering, 36 (2019) 92-100.

[6] Y. Zhang, J. Zhang, Y. Liu, Superhydrophobic surface with gamma irradiation resistance and self-cleaning effect in air and oil, Coatings, 10 (2020) 106.

[7] C. Lee, H. Kim, H.S. Ahn, M.H. Kim, J. Kim, Micro/nanostructure evolution of zircaloy surface using anodization technique: application to nuclear fuel cladding modification, Applied Surface Science, 258 (2012) 8724-8731.

[8] T.A. Otitoju, A.L. Ahmad, B.S. Ooi, Superhydrophilic (superwetting) surfaces: a review on fabrication and application, Journal of Industrial and Engineering Chemistry, 47 (2017) 19-40.

[9] X. Feng, L. Feng, M. Jin, J. Zhai, L. Jiang, D. Zhu, Reversible super-hydrophobicity to super-hydrophilicity transition of aligned ZnO nanorod films, Journal of the American Chemical Society, 126 (2004) 62-63.

[10] S. Wang, X. Feng, J. Yao, L. Jiang, Controlling wettability and photochromism in a dual-responsive tungsten oxide film Angewandte Chemie, 45 (2006) 1264-1267.

[11] G. Wang, T.Y. Zhang, Oxygen adsorption induced superhydrophilic-to-superhydrophobic transition on hierarchical nanostructured CuO surface, Journal of Colloid and Interface Science, 377 (2012) 438-441.

[12] X. Li, Y. Jiang, Z. Jiang, Y. Li, C. Wen, J. Lian, Reversible wettability transition between superhydrophilicity and superhydrophobicity through alternate heating-reheating cycle on laser-ablated brass surface, Applied Surface Science, 492 (2019) 349-361.

[13] T. Sun, G. Wang, F. L., B. Liu, Y. Ma, L. Jiang, D. Zhu, Reversible switching between superhydrophilicity and superhydrophobicity, Angewandte Chemie, 43 (2004) 357-360.

[14] D. Zhu, Z. Shi, X. Tan, J. Zhang, S. Zhang, X. Zhang, Accelerated wetting transition from hydrophilic to hydrophobic of sputtered Cu films with micro-scale patterns, Applied Surface Science, 527 (2020) 146741.

[15] F. Xia, Y. Zhu, L. Feng, L. Jiang, Smart responsive surfaces switching reversibly between super-hydrophobicity and super-hydrophilicity, Soft Matter, 5 (2009) 275-281.

[16] Y. Yu, N.M.A. Krishnan, M.M. Smedskjaer, G. Sant, M. Bauchy, The hydrophilic-to-hydrophobic transition in glassy silica is driven by the atomic topology of its surface, Journal of Chemical Physics, 148 (2018) 74503.

[17] C. Anitha, S.S. Azim, S. Mayavan, Fluorine free superhydrophobic surface textured silica particles and its dynamics-transition from impalement to impingment, Journal of Alloys and Compounds, 711 (2017) 197-204.

[18] S. Latthe, H. Imai, V. Ganesan, A.V. Rao, Superhydrophobic silica films by sol-gel co-precursor method, Applied Surface Science, 256 (2009) 217-222.

[19] X. Zhang, Y. Guo, P. Zhang, Z. Wu, Z. Zhang, Superhydrophobic and superoleophilic nanoparticle film: synthesis and reversible wettability switching behavior, ACS Applied Materials and Interfaces, 4 (2012) 1742-1746.

[20] X. Zhao, Y. Li, B. Li, T. Hu, Y. Yang, L. Li, J. Zhang, Environmentally benign and durable superhydrophobic coatings based on SiO_2 nanoparticles and silanes, Journal of Colloid and Interface Science, 542 (2019) 8-14.

[21] H. Ye, L. Zhu, W. Li, H. Liu, H. Chen, Construction fluorine-free and cost-effective superhydrophobic surface with normal-alcohol-modified hydrophobic SiO_2 nanoparticles, ACS Applied Materials and Interfaces, 9 (2017) 858-867.

[22] Y. Yan, Y. Cai, X. Li, G. Ma, W. Lv, M. Wang, Hydrophobic modication on the surface of SiO_2 nanoparticle: wettability control, Langmuir, 36 (2020) 14924-14932.

[23] Y. Cai, J. Li, L. Yi, X. Yan, J. Li, Fabricating superhydrophobic and eleophobic surface with silica nanoparticles modified by silanes and environment-friendly fluorinated chemicals, Applied Surface Science, 450 (2018) 102-111.

[24] S. Liu, X. Liu, S.S. Latthe, L. Gao, S. An, S.S. Yoon, L. B., R. Xing, Self-cleaning transparent superhydrophobic coatings through simple sol-gel processing of fluoralkylsinale, Applied Surface Science, 351 (2015) 897-903.

[25] Y. Wu, X. Li, C. Mi, L. Zong, X. Wang, Preparation and characterization of perfluorine-SiO_2 nanoparticles and superhydrophobic fluorosilicone/silica hybrid composite coating, Applied Physics A, 125 (2019) 250.

[26] X. Yang, H. Wang, P. Wang, X. Yang, H. Mao, Thermal stability of octadecyltrichlorosilane and perfluorooctyltriethoxysilane monolayers on SiO_2, Nanomaterials, 10 (2020) 210.

[27] J. Frechette, R. Maboudian, C. Carraro, Thermal behavior of perfluoroalkylsiloxane monolayers on the oxidized Si(100) surface, Langmuir, 22 (2006) 2726-2730.

[28] Q. Li, Y. Yan, M. Yu, B. Song, S. Shi, Y. Gong, Synthesis of polymeric fluorinated sol-gel precursor for fabrication of superhydrophobic coating, Applied Surface Science, 367 (2016) 101-108.

[29] K.Y. Law, Definitions for hydrophilicity, hydrophobicity, and superhydrophobicity: getting the basics right, Journal of Physical Chemistry Letters, 5 (2014) 686-688.

[30] A. Hozumi, K. Ushiyama, H. Sugimura, O. Takai, Fluoroalkylsilane monolayers formed by chemical vapor surface modification on hydroxylated oxide surfaces, Langmuir, 15 (1999) 7600-7604.

[31] P. Aminayi, N. Abidi, Ultra-oleaphobic cotton fabric prepared using molecular and nanoparticle vapor deposition methods Surface and Coatings Technology, 276 (2015) 636-644.

[32] M. Remezani, M.R. Vaezi, A. Kazemzadeh, Preparation of silane- functionalized silica films via two-step dip coating sol-gel and evaluation of their superhydrophobic properties Applied Surface Science, 317 (2014) 147-153.

[33] T. Diedrich, A. Dybowska, J. Schott, E. Valsami-Jones, E.H. Oelkers, The dissolution rates of SiO_2 nanoparticles as a function of particle size Environmental Science and Technology, 46 (2012) 4909-4915.

[34] T. Nishino, M. Meguro, K. Nakamae, M. Matsushita, Y. Ueda, The lowest surface free energy based on $-CF_3$ alignment, Langmuir, 15 (1999) 4321-4323.

[35] C. Pereira, C. Alves, A. Monteiro, C. Magen, A.M. Pereira, A. Ibarra, M.R. Ibarra, P.B. Tavares, J.P. Araujo, G. Blanco, J.M. Pintado, A.P. Carvalho, J. Pires, M.F.R. Pereira, C. Freire, Design novel hybrid materials by one-pot co-condensation: from hydrophobic mesoporous silica nanoparticles to superamphiphobic cotton textiles ACS Applied Materials and Interfaces, 3 (2011) 2289-2299.

[36] T. Monde, T. Kamiusuki, N. Nakayama, F. Nemoto, T. Yoko, T. Konakahara, Thermal decomposition of branched-polyfluoroalkylsilane coated on silica-gels Journal of the Ceramic Society of Japan, 104 (1996) 682-684.

[37] Z. Jiang, S. Fang, C. Wang, H. Wang, C. Ji, Durable polyorganosiloxane superhydrophobic films with a hierarchical structure by sol-gel and heat treatment method, Applied Surface Science, 390 (2016) 993-1001.

[38] K.L.S. Castro, S.M. Oliveira, R.V. Curti, J.R. Araujo, L.M. Sassi, C.M. Almeida, E.H.M. Ferreira, B.S. Archanjo, M.F. Cabral, A. Kuznetsov, L.A. Sena, C.A. Achete, E.D. Elia,

Electrochemical response of glassy carbon electrodes modified using graphene sheets of different sizes, International Journal of Electrochemical Science, 13 (2018) 71-87.

[39] K.H. An, J.G. Heo, K.G. Jeon, D.J. Bae, C. Jo, C.W. Yang, C.Y. Park, Y.H. Lee, X-ray photoemission spectroscopy sutdy of fluorinated single-walled carbon nanotubes, Applied Physics Letters, 80 (2002) 4235.

[40] A. Hozumi, O. Takai, Preparation of ultra water-repellent films by microwave plasma-enhanced CVD, Thin Solid Films, 303 (1977) 222-225.

[41] Y. Hattori, H. Kanoh, F. Okino, H. Touhara, D. Kasuya, M. Yudasaka, S. Lijima, K. Kaneko, Direct thermal fluorination of single wall carbon nanohorns, Journal of Physical Chemistry B, 108 (2004) 9614-9618.

[42] G. Nanse, E. Papirer, P. Fioux, F. Moguet, A. Tressaud, Fluorination of carbon blacks. An x-ray photoelectron spectroscopy study. Part II. XPS study of a furnace carbon black treated with gaseous fluorine at temperatures below 100 C. Influence of the reaction parameters and of the activation of the carbon black on the fluorine fixation, Carbon 35 (1997) 371-388.

[43] A.K. Chandra, M.T. Nguyen, T. Zeegers-Huyskens, Density functional calculations on simple carbonyl bases: protonation and hydrogen bond formation with water, Chemical Physics, 255 (2000) 149-163.

[44] L. Tam, D. Lau, C. Wu, Understanding interaction and dynamics of water molecules in the epoxy via molecular dynamics simulation, Molecular Simulation, 45 (2019) 120-128.

[45] Q. Zheng, C. Lu, Size effects of surface roughness to superhydrophobicity, Proceedia IUTAM 10 (2014) 462-475.

[46] B. Majhy, R. Iqbal, A.K. Sen, Facile fabrication and mechanistic understanding of a trasnaparent reversible superhydrophobic-superhydrophilic surface, Scientific Reports, 8 (2018) 18018.